

White Dwarfs as Dark Matter Detectors

Peter W. Graham,¹ Ryan Janish,² Vijay Narayan,² Surjeet Rajendran,² and Paul Riggins²

¹*Stanford Institute for Theoretical Physics, Department of Physics, Stanford University, Stanford, CA, 94305*

²*Berkeley Center for Theoretical Physics, Department of Physics,
University of California, Berkeley, CA 94720, USA*

If dark matter (DM) is capable of sufficiently heating a local region in a white dwarf, it will trigger runaway fusion and ignite a type Ia supernova. This was originally proposed in [4] and used to constrain primordial black holes which transit and heat a white dwarf via dynamical friction. In this paper, we extend the analysis of white dwarf DM detection to candidates with non-gravitational interactions that heat through the production of standard model (SM) particles. We consider a general class of models in which DM-DM collisions, DM decays, or DM transits including a SM scattering interaction produce particles that subsequently deposit energy inside the star. The existence of long-lived white dwarfs and the observed supernovae rate provide constraints for such models. As a concrete example, we rule out supersymmetric Q-ball DM in a large region of parameter space fundamentally inaccessible to terrestrial detection. It is also intriguing that the DM-induced ignition discussed in this work provide an alternative mechanism of triggering supernovae from sub-Chandrasekhar Mass progenitors.

Contents

I. Introduction	2
II. White Dwarf Runaway Fusion	2
III. Non-Gravitational Heating of White Dwarfs	4
A. High-Energy Showers	4
B. Low-Energy Elastic Heating	5
IV. Dark Matter-Induced Ignition	6
A. Classifying DM-WD Encounters	6
B. Transits	8
C. Collisions and Decays	9
V. Dark Matter Constraints	11
A. Review of WD Observables	12
B. Transit Constraints	12
C. Collision and Decay Constraints	13
VI. Q-balls	13
VII. Discussion	15
A. Particle Stopping in a White Dwarf	15
A. WD Medium	15
B. Nuclear Interactions	16
C. Radiative Processes	17
D. Elastic EM Scattering	17
Acknowledgements	19
References	19

I. INTRODUCTION

Identifying the nature of dark matter (DM) remains one of the clearest paths beyond the Standard Model (SM) and it is thus fruitful to study the observable signatures of any yet-allowed candidate. Many terrestrial direct detection experiments are designed to search for DM, e.g. [2, 3], yet these lose sensitivity to heavier DM due to its diminished number density. Even for a strongly-interacting candidate, if the DM mass is above $\sim 10^{22}$ GeV a detector of size $\sim (100 \text{ m})^2$ will register fewer than one event per year. While these masses are large compared to those of fundamental particles, it is reasonable to suppose that DM may exist as composite states just as the SM produces complex structures with mass much larger than fundamental scales (e.g. you, dear reader). Currently there is a wide range of unexplored parameter space for DM candidates less than $\sim 10^{48}$ GeV, above which the DM will have observable gravitational microlensing effects [1]. For such ultra-heavy DM, indirect signatures in astrophysical systems are a natural way forward. One possibility proposed by [4] is that DM can trigger runaway fusion and ignite type 1a supernovae (SN) in sub-Chandrasekhar white dwarf (WD) stars. This is even more interesting in light of recent observations that an $\mathcal{O}(1)$ fraction of type 1a SN are due to sub-Chandrasekhar progenitors [23, 24]. While astrophysical mechanisms for these events have been proposed [25, 26], the situation is yet unclear and it is an exciting possibility that these SN arise from DM interactions.

Runaway thermonuclear fusion requires both a heating event and the lack of significant cooling which might quench the process. The WD medium is particularly suited to this as it is dominated by degeneracy pressure and undergoes minimal thermal expansion, which is the mechanism that regulates fusion in main sequence stars. Thermal diffusion is the primary cooling process in a WD and it can be thwarted by heating a large enough region. The properties of a localized heating necessary to trigger runaway fusion were computed in [5]. Consequently, it was realized [4] that if DM is capable of sufficiently heating a WD in this manner, it will result in a SN with sub-Chandrasekhar Mass progenitor. This was used to constrain primordial black holes which transit a WD and cause heating by dynamical friction, although the authors of [4] identify several other heating mechanisms which may be similarly constrained.

In this paper, we examine DM candidates with non-gravitational interactions that cause heating through the production of SM particles. An essential ingredient in this analysis is understanding the length scales over which SM particles deposit energy in a WD medium. We find that most high energy particles thermalize efficiently with ions in the star, nearly independent of species or initial energy. Particle production is thus an effective means of heating WDs. Constraints on these DM candidates come from either observing specific, long-lived WDs or by comparing the measured rate of type 1a SN with that expected due to DM. It is important to note that these constraints are complementary to direct searches—it is more massive DM that is likely to trigger SN, but also more massive DM that has low terrestrial flux. The WD detector excels in this regime due to its large surface area $\sim (10^4 \text{ km})^2$, long lifetime $\sim \text{Gyr}$, and galactic abundance. We demonstrate these constraints for generic classes of DM models that produce SM particles via DM-DM collisions, DM decays, or DM transits including a SM scattering interaction. As a concrete example we consider ultra-heavy Q-ball DM as found in supersymmetric extensions of the SM.

The rest of the paper is organized as follows. We begin in Section ?? by reviewing the mechanism of runaway fusion in a WD. In Section ?? we study the non-gravitational heating of a WD due to the production of high-energy SM particles. Detailed calculations of the stopping of such particles are provided in Appendix A. In Section ?? we parameterize the explosiveness and event rate for generic classes of DM-WD encounters, and in Section V we derive schematic constraints on such models. Finally we specialize to the case of Q-balls in Section ??, and conclude in Section ??.

II. WHITE DWARF RUNAWAY FUSION

We first review the conditions for which a local energy deposition in a WD results in runaway fusion. Any energy deposit will eventually heat ions within some localized region—parameterize this region by its linear size L_0 , total kinetic energy \mathcal{E}_0 and typical temperature T_0 . These scales evolve in time, but it will be useful to describe a given heating event by their initial values.

The fate of a heated region is either a nonviolent diffusion of the excess energy across the star, or a runaway fusion chain-reaction that destroys the star. The precise outcome depends on L_0 , \mathcal{E}_0 and T_0 . There is a critical temperature T_f , set by the energy required for ions to overcome their mutual Coulomb barrier, above which fusion occurs. For carbon burning, $T_f \sim \text{MeV}$ [6]. Any heated region $T_0 > T_f$ will initially support fusion, although this is not sufficient for runaway as cooling processes may rapidly lower the temperature below T_f . This cooling will not occur if the corresponding timescale is larger than the timescale at which fusion releases energy. Cooling in a WD is dominated by thermal diffusion, and the diffusion time increases as the size of the heated region. However, the timescale for heating due to fusion is independent of region size. Thus, for a region at temperature $\gtrsim T_f$, there is a critical size above which the heated region does not cool but instead initiates runaway. For a region at the critical fusion temperature

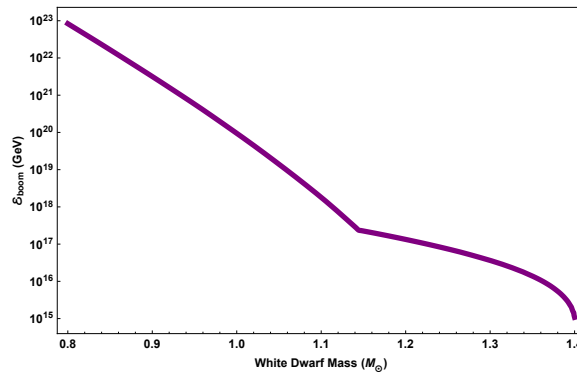


FIG. 1: The minimum energy deposit (2) necessary to trigger runaway fusion, based on numerical results for λ_T [5] and the WD mass-density relation [7]

T_f , we call this critical size the *trigger size* λ_T . The value of λ_T is highly dependent on density, and in a WD is set by the thermal diffusivity of either photons or degenerate electrons. This critical length scale has been computed numerically in [5] for a narrow range of WD densities and analytically scaled for other WD masses in [4]. As in [4], we will restrict our attention to carbon-oxygen WDs in the upper mass range $\sim 0.85 - 1.4 M_\odot$ (these will yield the most stringent constraints on DM). This corresponds to a central number density of ions $n_{\text{ion}} \sim 10^{30} - 10^{32} \text{ cm}^{-3}$ and a trigger size of $\lambda_T \sim 10^{-3} - 10^{-5} \text{ cm}$.

If a heated region is smaller than the trigger size, its thermal evolution is initially dominated by diffusion. However, this will still result in runaway fusion if the temperature is of order T_f by the time the region diffuses out to the trigger size. For our purposes it is more natural to phrase this in terms of the total energy \mathcal{E}_0 deposited during a heating event. Of course, the relation between energy \mathcal{E}_0 and temperature T_0 depends on the rate at which WD constituents—ions, electrons, and photons—thermalize with each other within the region size L_0 . In Section ?? we explicitly calculate the length scales over which a hot bath of ions thermalizes electrons and photons, focusing our attention on ions because they are what ultimately must be heated in order for fusion to take place. Here we simply state the results: if ions are heated to temperatures $T_0 \sim 1 - 10 \text{ MeV}$, typical for a wide variety of heating processes, then electrons and photons are also heated to T_0 within the trigger size. Therefore, any heating event which results in runaway necessarily has ions, electrons, and photons in thermal equilibrium once a region of size λ_T or greater is at the critical temperature T_f . The excess energy in a volume V required to heat all these species to T_f is given by a sum of their heat capacities

$$\frac{\mathcal{E}_0}{V} \gtrsim \int_0^{T_f} dT (n_{\text{ion}} + n_e^{2/3} T + T^3), \quad (1)$$

where n_e is the number density of electrons. Note that we use the heat capacity of a degenerate gas of electrons, since the Fermi energy $E_F \gtrsim \text{MeV}$ for the densities we consider. The minimum energy deposit necessary to trigger runaway fusion is simply

$$\begin{aligned} \mathcal{E}_{\text{boom}} &\sim \lambda_T^3 (n_{\text{ion}} T_f + n_e^{2/3} T_f^2 + T_f^4) \\ &\approx 10^{15} - 10^{23} \text{ GeV}. \end{aligned} \quad (2)$$

$\mathcal{E}_{\text{boom}}$ varies with λ_T over the range of WD densities and is plotted in Figure 1. Thus for a heating event characterized by its L_0 , \mathcal{E}_0 , and $T_0 \gtrsim T_f$, there is a *boom condition*:

$$\mathcal{E}_0 \gtrsim \mathcal{E}_{\text{boom}} \cdot \max \left\{ 1, \frac{L_0}{\lambda_T} \right\}^3. \quad (3)$$

Any \mathcal{E}_0 satisfying this condition is minimized for L_0 less than the trigger size, where it is also independent of the precise value of L_0 . For broader deposits, the necessary energy is parametrically larger than $\mathcal{E}_{\text{boom}}$ by a volume ratio $(L_0/\lambda_T)^3$. As a result, understanding the L_0 for different kinds of heating events in a WD is critical to determining whether or not they are capable of destroying the star.

III. NON-GRAVITATIONAL HEATING OF WHITE DWARFS

We address now the possibility of DM heating the WD medium via the production of SM particles. The critical quantity is the length scale over which such SM particles heat the medium—this scale determines their efficiency in triggering runaway fusion as described by condition (3). Note that this is a question of purely SM physics. The unknown physics of DM will serve only to set the initial properties of the SM particles.

One may have expected that efficient heating occurs only for a limited range of SM species and energies, thus restricting the set of DM candidates capable of producing SN. However, we find that SM particles tend to efficiently heat the WD regardless of species or energy—the length scale of heating is typically less than or of order the trigger size λ_T , and is never parametrically larger. This is accomplished primarily through hadronic showers initiated by collisions with carbon ions. In some cases electromagnetic shower processes are important, however at high energies these are suppressed by density effects and photons/electrons are dominated by hadronic interactions. These interactions rapidly stop high-energy particles due to the logarithmic nature of showers, converting them into a cloud of low-energy particles which efficiently heat the WD medium through elastic scatters. In this light, the WD operates analogously to a particle detector, including hadronic and electromagnetic “calorimeter” components. Runaway fusion provides the necessary amplification to convert a detected event into a recordable signal, in this case a violent SN.

In the remainder of this section we present the above heating process in detail. We summarize the dominant source of energy loss and the resulting stopping lengths λ for SM particles of incident kinetic energy ϵ , approximated by

$$\lambda \sim \frac{\epsilon}{dE/dx}, \quad (4)$$

where dE/dx is the stopping power in the WD medium. These are plotted in Figures 2, 3, 4, and 5. A detailed treatment of the stopping powers is reserved for Appendix A. We will consider incident light hadrons, photons, electrons, and neutrinos—as we are concerned with triggering runaway fusion, we restrict our attention to energies $\epsilon \gg T_f \sim \text{MeV}$. A schematic for this flow of energy deposition is given in Figure ??.

A. High-Energy Showers

a. Hadronic Showers. Incident hadrons with kinetic energy larger than the nuclear binding scale $E_{\text{nuc}} \sim 10 \text{ MeV}$ will undergo violent inelastic collisions with carbon ions resulting in an $\mathcal{O}(1)$ number of secondary hadrons. This results in a roughly collinear shower of hadrons which ends when the constituents reach an energy $\sim E_{\text{nuc}}$. This occurs over a shower length

$$X_{\text{had}} \sim l_{\text{inel}} \log \left(\frac{\epsilon}{E_{\text{nuc}}} \right) \approx 10^{-6} \text{ cm} \left(\frac{10^{32} \text{ cm}^{-3}}{n_{\text{ion}}} \right) \quad (5)$$

where l_{inel} is the mean free path for nuclear scatters, set by $\sigma_{\text{inel}} \approx 100 \text{ mb}$, and we have taken the logarithm to be ~ 10 . The shower terminates into an exponential number of $\sim 10 \text{ MeV}$ hadrons with roughly equal fractions of pions, protons, and neutrons. For a more detailed discussion of hadronic showers, see Appendix AB. Note that neutral pions of energy $10 - 100 \text{ MeV}$ have a decay length to photons of order $\delta_{\pi^0} \sim 10^{-6} \text{ cm}$. Hadronic showers will therefore generate an electromagnetic component carrying an $\mathcal{O}(1)$ fraction of the energy.

b. Photonuclear and Electronuclear Showers. The LPM effect (see next section) ensures that hadronic interactions become important at sufficiently high energies even for electrons and photons. Photons can interact hadronically via quark-antiquark pairs and directly induce hadronic showers off ions. The only quantitative difference between these showers and purely hadronic ones is that they require a slightly longer distance to initiate. Roughly, the photonuclear cross section is suppressed relative to the hadronic inelastic cross section by a factor of α required to produce a quark-antiquark pair. This gives a photon range

$$\lambda_{\gamma A} \sim \frac{l_{\text{inel}}}{\alpha} \approx 10^{-5} \text{ cm} \left(\frac{10^{32} \text{ cm}^{-3}}{n_{\text{ion}}} \right). \quad (6)$$

Note that $\lambda_{\gamma A}$ is the distance to begin a hadronic shower, whereas the shower itself extends a distance X_{had} .

In the regime of strong LPM suppression, high-energy electrons will also initiate hadronic showers through virtual photons. This process is best described as a continuous energy loss of the electron into minimal $\sim 10 \text{ MeV}$ hadronic showers. The electronuclear stopping length is

$$\lambda_{eA} \approx 10^{-4} \text{ cm} \left(\frac{10^{32} \text{ cm}^{-3}}{n_{\text{ion}}} \right). \quad (7)$$

This is suppressed by an additional factor of α relative to the photonuclear interaction, however a full calculation also yields an $\mathcal{O}(10)$ logarithmic phase-space enhancement. For electron energies greater than $\sim 10^6 - 10^8$ GeV (depending on the WD density), electronuclear stopping even dominates over the bremsstrahlung of real photons that then interact hadronically.

c. Electromagnetic Showers. Of course, electrons and photons also shower through successive bremsstrahlung and pair-production interactions. An EM shower proceeds until a critical energy ~ 100 MeV set by the scale at which these radiative processes become subdominant to Coulomb and Compton scattering. Below this scale radiation can still be important, though EM showers do not occur. Note that bremsstrahlung and pair-production are strictly forbidden for incident energies below the electron Fermi energy.

At sufficiently high electron/photon energies and nuclear target densities, EM showers are elongated due to the “Landau-Pomeranchuk-Migdal” (LPM) effect. High-energy radiative processes necessarily involve small momentum transfers to nuclei. These soft virtual photons cannot be exchanged with only a single ion, but rather interact simultaneously with multiple ions. This generates a decoherence, suppressing bremsstrahlung/pair-production above an energy E_{LPM} which scales inversely with density:

$$E_{\text{LPM}} \approx 1 \text{ MeV} \left(\frac{10^{32} \text{ cm}^{-3}}{n_{\text{ion}}} \right) \quad (8)$$

The corresponding shower lengths are

$$X_{\text{EM}} \approx X_0 \cdot \begin{cases} \left(\frac{\epsilon}{E_{\text{LPM}}} \right)^{1/2} & \epsilon > E_{\text{LPM}} \\ 1 & \epsilon < E_{\text{LPM}} \end{cases} \quad (9)$$

where

$$X_0 \approx 10^{-7} \text{ cm} \left(\frac{10^{32} \text{ cm}^{-3}}{n_{\text{ion}}} \right). \quad (10)$$

See Appendix A C for further details. At the highest WD densities radiative processes are always LPM-suppressed, while at lower densities we observe both regimes. In high-density WDs, EM showers completely carry the energy of $\sim 10^2 - 10^4$ MeV electrons and photons. The lower end of this range corresponds to the scale at which elastic scatters dominate, and the upper end corresponds to the scale at which photonuclear interactions dominate.

d. Neutrino-induced Showers Neutrinos scatter off ions with a cross section that increases with energy. In these interactions, an $\mathcal{O}(1)$ fraction of the neutrino energy is transferred to the nucleus with the rest going to produced leptons [8]—this is sufficient to start a hadronic shower. At an energy of $\sim 10^{11}$ GeV, neutrino-nuclear cross section is determined [8] to be $\sim 10^{-32} \text{ cm}^2$, which we will conservatively take as an estimate for even higher energies. This gives a distance of order \sim meter for a neutrino to initiate a hadronic shower. While it is much too large to efficiently heat a WD via the release of multiple neutrinos, the neutrino mean free path is simply the displacement for a single high-energy neutrino to begin a shower of size X_{had} —this is qualitatively similar to the photonuclear length (6). As such, a single ultra-high energy neutrino released in the WD can efficiently heat the star.

B. Low-Energy Elastic Heating

The showers of high-energy particles described above terminate in a cloud of low-energy $\epsilon \sim 10$ MeV neutrons, protons, and charged pions, and $\epsilon \sim 100$ MeV electrons and photons. Of course, particles at these energies may also be directly produced by the DM. At these energies, Coulomb, Compton, and elastic nuclear scatters dominate and eventually lead to the thermalization of ions. The stopping powers for these processes are calculated in the Appendix.

a. Nucleons and Pions. Neutrons and neutral pions are the simplest species we consider, interacting at low-energies only through elastic nuclear scatters characterized by a cross section $\sigma_{\text{el}} \approx b$, enhanced from the inelastic interaction by a factor of ~ 10 . Note that the mass hierarchy between these particles and the ions requires $\sim 10 - 100$ scatters to transfer the hadron’s energy in the form of a random-walk. This elastic heating range is approximately

$$\lambda_{\text{el}} \approx 10^{-7} \text{ cm} \left(\frac{10^{32} \text{ cm}^{-3}}{n_{\text{ion}}} \right), \quad (11)$$

and is always less than the trigger size. Note that this may or may not be shorter than the neutral pion decay length δ_{π^0} , depending on the WD density. Low-energy neutrons thus always provide efficient heating, low-energy neutral

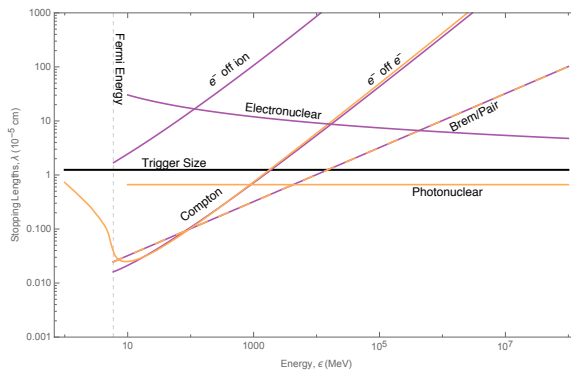


FIG. 2: Stopping lengths of incident photons and electrons as a function of kinetic energy in a WD of density $n_{\text{ion}} \sim 10^{32} \text{ cm}^{-3}$ ($\approx 1.37 M_{\odot}$). Orange lines are incident photons, purple lines are incident electrons. The dashed line is the EM shower length X_{EM} .

pions provide efficient heating at high densities, and the effectiveness of neutral pions at low densities depends on the stopping of $\approx 70 \text{ MeV}$ photons. We now turn to charged hadrons, which are subject to Coulomb interactions with ions and electrons as well as elastic nuclear scatters similar to their neutral brethren. At energies $\epsilon \lesssim 10 \text{ MeV}$, scattering off electrons is in fact the least dominant of these processes, contrary to the behavior of terrestrial detectors. This is due to the significant Pauli-blocking of electron interactions near the Fermi energy $E_F \sim 1 - 10 \text{ MeV}$. Low-energy charged hadrons will thus predominantly lose energy through elastic nuclear scatters or in a small range of energies, Coulomb scatters off ions—either way, both interactions length scales are well below the trigger size and transfer energy to ions. In the context of a hadronic shower, the final-state hadrons are $\sim 10 \text{ MeV}$ nucleons and pions, with each species carrying an $\mathcal{O}(1)$ fraction of the initial energy. These products will thermalize within a trigger size and thus hadronic showers are also an efficient heating mechanism.

b. Electrons and Photons. As shown in Figures 2 and 3, electron stopping at low energy is dominated by bremsstrahlung and photon stopping by Compton scatters. Thus, at these energies electrons and photons first thermalize into a compact electromagnetic “gas” of size $X_{\text{EM}} < \lambda_T$. This gas cools and diffuses to larger length scales, eventually allowing subdominant processes to thermalize carbon ions. The details of this evolution depend on the initial EM gas temperature T , which is set by the total SM energy released by the DM. If the gas is below 10 MeV before the photonuclear scale, the dominant process will be Coulomb scattering of hot electrons off WD ions. We have checked that this is the case for any EM cloud formed from the final-state products of high-energy electromagnetic showers. Note that for temperatures T less than the Fermi energy, the electrons are partially degenerate and heating proceeds via the thermal tail with kinetic energies $\epsilon \sim E_F + T$. We calculate this stopping length is roughly of order but slightly larger than the trigger size. The fact that this length scale is larger than the trigger size simply means that constraints relying on this specific heating process will have some volume dilution, increasing the necessary energy deposit according to (3). If instead the gas remains above 10 MeV by the time it has diffused to a size $\lambda_{\gamma A}$, the photons in the gas will efficiently thermalize ions via photonuclear showers and subsequent nuclear elastic heating (see discussion above).

IV. DARK MATTER-INDUCED IGNITION

The unknown physics of DM sets the rate of SM particle production within the star as well as the initial distribution in space, momentum, and species of the products. This information is needed to determine if a given DM encounter with a WD results in runaway fusion and with what frequency. Of course, this can be done precisely for a specific DM model. In this Section, we describe several general, illustrative classes of DM-WD encounters which demonstrate the explosiveness of ultra-heavy DM interactions. We also calculate the typical rates at which these events take place in a WD.

A. Classifying DM-WD Encounters

DM can generically heat the WD medium through the three schematic interactions depicted in Figure 6: DM-DM collisions, DM decays, and DM-SM scattering. Note that for ultra-heavy DM these can be complicated events involving

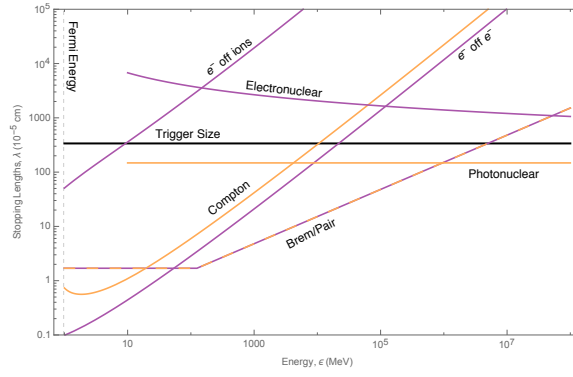


FIG. 3: Stopping lengths of incident photons and electrons as a function of kinetic energy in a WD of density $n_{\text{ion}} \sim 10^{30} \text{ cm}^{-3}$ ($\approx 0.85 M_{\odot}$). Orange lines are incident photons, purple lines are incident electrons. The dashed line is the EM shower length X_{EM} .

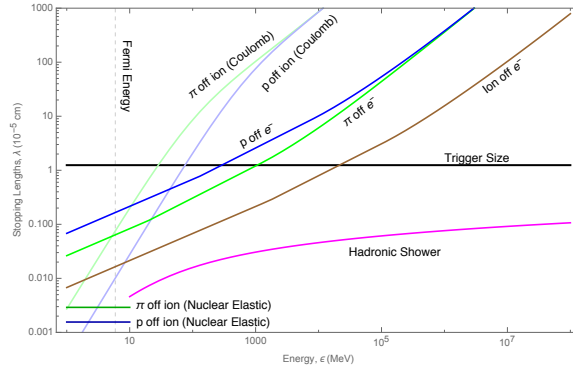


FIG. 4: Stopping lengths for incident hadrons as a function of kinetic energy in a WD of density $n_{\text{ion}} \sim 10^{32} \text{ cm}^{-3}$ ($\approx 1.37 M_{\odot}$). The magenta line is the hadronic shower length X_{had} .

many (possibly dark) final states, analogous to the interactions of heavy nuclei. We classify DM candidates into three types according to the interaction that provides the dominant source of heating, and refer to these as collision, decay, and transit candidates. We additionally make simplifying assumptions about the spatial extent of these interactions. For collisions and decays, we consider only “point-like” heating events with all SM products produced in a localized region (smaller than the trigger size). For transits, we consider only DM-SM scatters that result in a continuous release of particles along the DM trajectory.

We can also classify candidates according to the evolution of the DM itself inside the star. Generally there will be

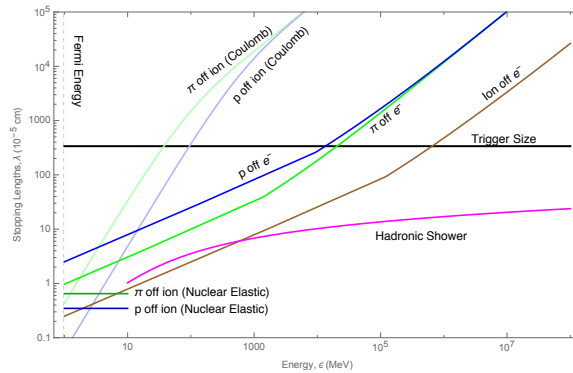


FIG. 5: Stopping lengths for incident hadrons as a function of kinetic energy in a WD of density $n_{\text{ion}} \sim 10^{30} \text{ cm}^{-3}$ ($\approx 0.85 M_{\odot}$). The magenta line is the hadronic shower length X_{had} .

some loss of DM kinetic energy due to DM-SM scatters—this is either incidental to the eventual heating of the star or represents the dominant heating mechanism. We consider two simple, limiting cases depending on the magnitude of this energy loss relative to the DM kinetic energy: “DM wind” and “DM capture”. In the DM wind scenario, there is negligible energy loss and the DM simply passes through the star. In the DM capture scenario, the energy loss due to DM-SM scatters is not capable of igniting runaway but is sufficient to stop the DM and cause it to accumulate inside the star. We consider both scenarios for collision and decay candidates, for which the capture results in a significantly enhanced rate of events. For simplicity we consider only the wind scenario for transit candidates, though an enhanced explosiveness from slowed DM continuously scattering off stellar constituents is certainly possible in some models.

B. Transits

a. Ignition Condition. Runaway fusion only occurs in the degenerate WD interior where thermal expansion is suppressed as a cooling mechanism. The outer layers of the WD, however, are composed of a non-degenerate gas and it is therefore essential that a DM candidate penetrate this layer in order to ignite a SN. We parameterize this by a DM stopping power $(dE/dx)_{\text{SP}}$, the kinetic energy lost by the DM per distance traveled in the non-degenerate layer, and demand that

$$\left(\frac{dE}{dx}\right)_{\text{SP}} \ll \frac{m_\chi v_{\text{esc}}^2}{R_{\text{env}}}, \quad (12)$$

where $R_{\text{env}} \sim 50$ km is the width of a WD envelope [35].

The energy deposited during a continuous heating event such as a DM transit is best described in terms of a linear energy transfer $(dE/dx)_{\text{LET}}$, the kinetic energy of SM particles produced per distance traveled by the DM. If these products have a heating length L_0 then the relevant energy deposit must at minimum be taken as the energy transferred over the transit distance L_0 . Of course, we can always choose to consider energy deposits over a longer segment of the DM trajectory. Importantly, as per the general condition (3) such a deposition is *less* explosive unless L_0 is smaller than the trigger size λ_T . Thus, we consider the energy deposited in a transit over the larger of these two length scales. Assuming the energy of the DM is roughly constant over this heating event, the ignition condition for transit heating is:

$$\left(\frac{dE}{dx}\right)_{\text{LET}} \gtrsim \frac{\mathcal{E}_{\text{boom}}}{\lambda_T} \cdot \max\left\{\frac{L_0}{\lambda_T}, 1\right\}^2. \quad (13)$$

Note that the DM stopping power in the non-degenerate layer $(dE/dx)_{\text{SP}}$ and the linear energy transfer in the degenerate interior $(dE/dx)_{\text{LET}}$ are possibly controlled by different physics and may have very different numerical values. In addition, a transit heating event satisfying condition (12) will have negligible energy loss over the parametrically smaller trigger size or heating length L_0 , validating (13).

The above argument sums the individual energy deposits along the DM trajectory as though they are all deposited simultaneously. This is possible if the DM moves sufficiently quickly so that this energy does not diffuse out of the region of interest before the DM has traversed the region. We therefore require that the diffusion time $\tau_{\text{diff}} \sim 10^{-12}$ s across a heated region at temperature T_f be larger than the DM crossing-time:

$$\tau_{\text{diff}} \sim \frac{L^2}{\alpha(T_f)} \gg \frac{L}{v_{\text{esc}}}, \quad (14)$$

where $\alpha(T)$ is the temperature-dependent diffusivity, and the DM transits at the stellar escape velocity $v_{\text{esc}} \sim 10^{-2}$. This condition is more stringent for smaller regions, so we focus on the smallest region of interest, $L = \lambda_T$. (14) is then equivalent to demanding that the escape speed is greater than the conductive speed of the fusion wave front, $v_{\text{cond}} \sim \alpha(T_f)/\lambda_T$. Numerical calculations of v_{cond} are tabulated in [5], and indeed condition (14) is satisfied for all WD densities.

b. Event Rate: Wind Scenario. The rate of transit events is given by the flux of DM passing through a WD

$$\Gamma_{\text{trans}} \sim \frac{\rho_\chi}{m_\chi} R_{\text{WD}}^2 \left(\frac{v_{\text{esc}}}{v_{\text{halo}}}\right)^2 v_{\text{halo}}, \quad (15)$$

where ρ_χ is the DM density in the region of the WD, and R_{WD} is the WD radius. Here $v_{\text{halo}} \sim 10^{-3}$ is the virial velocity of our galactic halo, and the transit rate contains an $(v_{\text{esc}}/v_{\text{halo}})^2 \sim 100$ enhancement due to gravitational focusing.

C. Collisions and Decays

a. Ignition Condition. For a point-like DM-DM collision or DM decay event releasing particles of heating length L_0 , ignition will occur if the total energy in SM products satisfies condition (3). Such an event will likely result in both SM and dark sector products, so we parameterize the resulting energy in SM particles as a fraction f_{SM} of the DM mass. For non-relativistic DM, the DM mass is the dominant source of energy and therefore $f_{\text{SM}} \lesssim 1$ regardless of the interaction details. With this parameterization, a single DM-DM collision or DM decay has an ignition condition:

$$m_\chi f_{\text{SM}} \gtrsim \mathcal{E}_{\text{boom}} \cdot \max \left\{ \frac{L_0}{\lambda_T}, 1 \right\}^3. \quad (16)$$

We are thus sensitive to DM masses $m_\chi \gtrsim 10^{16}$ GeV.

b. Event Rate: DM Wind. DM that is not captured traverses the WD in $R_{\text{WD}}/v_{\text{esc}}$, and the rate of DM-DM collisions within the WD parameterized by cross-section $\sigma_{\chi\chi}$ is:

$$\Gamma_{\text{ann}} \sim \left(\frac{\rho_\chi}{m_\chi} \right)^2 \sigma_{\chi\chi} \left(\frac{v_{\text{esc}}}{v_{\text{halo}}} \right)^3 v_{\text{halo}} R_{\text{WD}}^3. \quad (17)$$

Similarly the net DM decay rate inside the WD parameterized by a lifetime τ_χ is:

$$\Gamma_{\text{decay}} \sim \frac{1}{\tau_\chi} \frac{\rho_\chi}{m_\chi} \left(\frac{v_{\text{esc}}}{v_{\text{halo}}} \right) R_{\text{WD}}^3. \quad (18)$$

c. Event Rate: DM Capture. For the remainder of this section, all numerical quantities are evaluated assuming a central WD density $n_{\text{ion}} \sim 10^{31} \text{ cm}^{-3}$. At this density, the relevant WD parameters are approximately:

$$M_{\text{WD}} \sim 1.25 M_\odot, \quad R_{\text{WD}} \sim 4000 \text{ km}, \quad v_{\text{esc}} \sim 2 \times 10^{-2}. \quad (19)$$

We also assume a typical WD temperature $T \sim \text{keV}$.

For the DM to be captured in a WD, it must lose energy $\sim m_\chi v^2$, where v is the relative DM velocity (in the rest frame of the WD) asymptotically far away. Properly, this DM velocity is described by a (boosted) Maxwell distribution peaked at the galactic virial velocity $v_{\text{halo}} \sim 10^{-3}$. Since typically $v \ll v_{\text{esc}}$, the DM has initial velocity v_{esc} in the star and must lose a fraction $(v/v_{\text{esc}})^2$ of its energy to become captured. The physics of DM capture can be made more precise for a specific interaction. Consider a spin-independent, elastic scattering off ions with cross section $\sigma_{\chi A}$. Assuming $m_{\text{ion}} \ll m_\chi$, the typical momentum transfer in an elastic scatter is $q \sim \mu_A v_{\text{esc}} \sim 200 \text{ MeV}$, where $\mu_A \sim m_{\text{ion}}$ is the reduced mass of the DM-nuclei system. This corresponds to an energy transfer $q^2/m_{\text{ion}} \sim m_{\text{ion}} v_{\text{esc}}^2 \sim 10 \text{ MeV}$. The average number of DM scatters during a full transit of the WD is simply a ratio of the mean free path to the size of the WD

$$\bar{N}_{\text{scat}} \sim n_{\text{ion}} \sigma_{\chi A} R_{\text{WD}}. \quad (20)$$

If $\bar{N}_{\text{scat}} < 1$, then \bar{N}_{scat} is the probability for a *single* scatter to occur during the transit.

The capture of DM in gravitating bodies is very well-studied [?]. This calculation becomes slightly involved if a single scatter is ever insufficient to capture the DM. For incoming DM with asymptotic velocity $\sim v_{\text{halo}}$ (the peak of the Maxwell distribution), multiple scatters are required if

$$B \equiv \frac{m_{\text{ion}} v_{\text{esc}}^2}{m_\chi v_{\text{halo}}^2} \lesssim 1. \quad (21)$$

It can be shown that the general rate of capture is approximately of the form

$$\Gamma_{\text{cap}} \sim \Gamma_{\text{trans}} \cdot \min \{ 1, \bar{N}_{\text{scat}} \min \{ B, 1 \} \}. \quad (22)$$

Evidently, the assumption that the scatters responsible for slowing the DM are not sufficient to blow up the WD (13) is a valid one for cross sections

$$\sigma_{\chi A} < \left(\frac{\mathcal{E}_{\text{boom}}}{\lambda_T} \right) \left(\frac{1}{m_{\text{ion}} v_{\text{esc}}^2} \right) \left(\frac{1}{n_{\text{ion}}} \right) \sim 10^{-8} \text{ cm}^2, \quad (23)$$

Since the momentum transfer $q \sim 100$ MeV is of order the inverse nuclear size, it is reasonable to expect the DM coherently scatters off all nucleons in any nucleus. The average per-nucleon cross section (spin-independent) is given by

$$\sigma_{\chi A} = A^2 \left(\frac{\mu_A}{\mu_n} \right)^2 F^2(q) \sigma_{\chi n} \sim A^4 F^2(q) \sigma_{\chi n}, \quad (24)$$

where $F^2(q)$ is the Helm form factor [?]:

$$F^2(q) = \exp(-q^2 s^2) \left(\frac{3j_1(qR_n)}{qR_n} \right)^2, \quad s \sim \text{fm}, \quad R_n \sim \sqrt{(A^{1/3})^2 - 5s}. \quad (25)$$

For momentum transfers at a DM velocity v_{esc} , we find that $F^2(q) \sim 0.1$. In general, the form factor should range from $F^2 \sim 10^{-2} - 1$, where for sufficiently q the DM is effectively scattering off individual nucleons. We will conservatively take $F^2 \sim 0.1$ for all momentum transfers, and this does not affect the results significantly. Currently, the bound on spin-independent DM nuclear elastic scatters from XENON 1T [?] is

$$\sigma_{\chi n} < 10^{-45} \text{ cm}^2 \left(\frac{m_\chi}{10^3 \text{ GeV}} \right). \quad (26)$$

Interestingly, any DM candidate whose scattering cross section satisfies the direct detection constraint is necessarily capturing only a fraction 10^{-2} or fewer of those DM which transit the star. Therefore, we are in the regime where capture rate has the following parametric dependence on mass and scattering cross section:

$$\Gamma_{\text{cap}} \propto \frac{\sigma_{\chi A}}{m_\chi^2}. \quad (27)$$

First we review the evolution of captured DM in the WD ignoring DM collisions or decays. Once DM is captured, it eventually thermalizes to an average velocity

$$v_{\text{th}} \sim \sqrt{\frac{T}{m_\chi}} \sim 10^{-12} \left(\frac{m_\chi}{10^{16} \text{ GeV}} \right)^{-1/2} \quad (28)$$

and settles at the thermal radius

$$R_{\text{th}} \sim \left(\frac{T}{Gm_\chi \rho_{\text{WD}}} \right)^{1/2} \sim 0.1 \text{ cm} \left(\frac{m_\chi}{10^{16} \text{ GeV}} \right)^{-1/2}, \quad (29)$$

where its kinetic energy balances against the gravitational potential energy of the (enclosed) WD mass (for simplicity, we take a constant WD density $\rho_{\text{WD}} \sim n_{\text{ion}} m_{\text{ion}}$ within R_{th}). Of course, the timescale for thermalization depends on the nature of the DM-SM interaction. This has been explicitly calculated in the case that the DM loses energy via elastic nuclear scatters, see [?]. First, the DM passes through the WD many times before the size of its orbit becomes fully contained within the star. This occurs after a time

$$t_1 \sim \left(\frac{m_\chi}{m_{\text{ion}}} \right)^{3/2} \frac{R_{\text{WD}}}{v_{\text{esc}}} \frac{1}{\bar{N}_{\text{scat}}} \frac{1}{\max\{\bar{N}_{\text{scat}}, 1\}^{1/2}} \sim 7 \times 10^7 \text{ s} \left(\frac{m_\chi}{10^{16} \text{ GeV}} \right)^{3/2} \left(\frac{\sigma_{\chi A}}{10^{-30} \text{ cm}^2} \right)^{-3/2}. \quad (30)$$

This stage is relevant only if the energy loss after a single transit does not exceed $\sim m_\chi v_{\text{esc}}^2$

$$\left(\frac{m_{\text{ion}}}{m_\chi} \right) \max\{\bar{N}_{\text{scat}}, 1\} < 1, \quad (31)$$

which is the case for any cross sections which satisfy the XENON bound (26). Subsequently, the DM completes many orbits within the star until dissipation from elastic scatters reduces the orbital size to the thermal radius. This occurs after a time

$$t_2 \sim \left(\frac{m_\chi}{m_{\text{ion}}} \right) \frac{1}{n_{\text{ion}} \sigma_{\chi A}} \frac{1}{v_{\text{ion}}} \left\{ 1 + \log \left(\frac{m_\chi}{m_{\text{ion}}} \right) \right\} \sim 3 \times 10^8 \text{ s} \left(\frac{m_\chi}{10^{10} \text{ GeV}} \right) \left(\frac{\sigma_{\chi A}}{10^{-38} \text{ cm}^2} \right)^{-1}. \quad (32)$$

where $v_{\text{ion}} \sim \sqrt{\frac{T}{m_{\text{ion}}}}$. Note that the time to complete a single orbit is simply the free-fall timescale:

$$t_{\text{ff}} \sim \sqrt{\frac{1}{G\rho_{\text{WD}}}} \sim 0.1 \text{ s}. \quad (33)$$

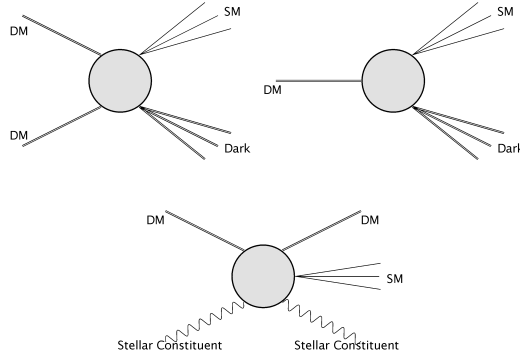


FIG. 6: Schematic of possible non-gravitational DM interactions in a WD which release SM (and possibly dark sector) particles.

If the settling time $t_1 + t_2$ is less than the age of the WD, then the DM will begin steadily accumulating at R_{th} . However, if the collected mass of DM at the thermal radius ever exceeds the WD mass within this volume, then there is the possibility of self-gravitational collapse of the DM. The time to collect a critical number of DM particles needed for self-gravitation is given by

$$t_{\text{sg}} \sim \frac{\rho_{\text{WD}} R_{\text{th}}^3}{m_\chi \Gamma_{\text{cap}}} \sim 10^4 \text{ s} \left(\frac{m_\chi}{10^{16} \text{ GeV}} \right)^{-1/2} \left(\frac{\sigma_{\chi A}}{10^{-30} \text{ cm}^2} \right)^{-1} \dots \quad (34)$$

We now turn towards the rate of DM-DM collisions during various stages of the described evolution. After a time t_1 , the settling DM constitutes a number density throughout the WD volume. The total rate of annihilations of this DM population is given by:

$$\Gamma_{\text{ann}} \sim \Gamma_{\text{cap}}^2 \left(\frac{R_{\text{WD}}}{R_{\text{th}}} \right)^2 \sigma_{\chi\chi} \frac{m_\chi}{\sigma_{\chi A}} \frac{G}{R_{\text{th}}^2 v_{\text{esc}} v_{\text{ion}}^2}. \quad (35)$$

Even if the annihilation rate for infalling DM is too small, a complementary constraint can be derived from DM-DM collisions at the thermal radius. As this population of DM only lasts for a time t_{sg} , the condition that a single collision does not occur before self-gravitation is:

$$\frac{(\Gamma_{\text{cap}} t_{\text{sg}})^2}{R_{\text{th}}^3} \sigma_{\chi\chi} v_{\text{th}} t_{\text{sg}} < 1. \quad (36)$$

At this point, the DM sphere will start to shrink. The ability for a self-gravitating DM sphere to ignite the WD via annihilations is especially interesting. Such a process yields novel bounds that also extend to lower DM masses, and will be discussed in detail in forthcoming work [?].

Finally, we compute the decay rate of captured DM. Of course, this rate is proportional to the number of DM particles within the WD at any given instance. In the wind scenario (18), this number is given by $\sim (\Gamma_{\text{trans}} \times t_{\text{ff}})$. In the capture scenario, the number of DM particles available for decay is instead determined by the settling time inside the WD?

$$\Gamma_{\text{decay}} \sim \frac{1}{\tau_\chi} \Gamma_{\text{cap}} t_2 \quad (37)$$

Since, (37) is independent of $\sigma_{\chi A}$ and scales inversely with m_χ , the rate of captured DM decays in the WD is simply enhanced by a factor $\sim \left(\frac{v_{\text{esc}}^3}{v_{\text{halo}}^2 v_{\text{ion}}} \right) \sim 10^5$ compared to the rate of transiting “wind” decays (18).

V. DARK MATTER CONSTRAINTS

We now constrain some simplified models of DM which will ignite a WD via one of the processes parameterized in Section IV. First, however, we review how WD observables constrain DM candidates capable of triggering SN.

A. Review of WD Observables

Following the discussion of [4], our constraints come from (1) the existence of heavy, long-lived white dwarfs, or (2) the measured type Ia SN rate. The typical age of a WD is of order the age of the universe \sim Gyr. RX J0648.04418 is a nearby star and one of the heavier known WDs, with a mass $\sim 1.25 M_\odot$ [10] and local dark matter density which we will take to be $\rho_\chi \sim 0.4 \text{ GeV/cm}^3$. Of course, this is not the only known heavy WD—the Sloan Digital Sky Survey [11] has found 20+ others. The NuStar collaboration has also recently uncovered evidence for the likely existence of $\sim 1.25 M_\odot$ WDs in the galactic center [12], where it is estimated that $\rho_\chi \sim 10^3 \text{ GeV/cm}^3$ [13]. Such heavy candidates are particularly suited for our constraints as the energy deposit necessary to trigger SN $\mathcal{E}_{\text{boom}}$ is a decreasing function of WD mass. However, less dense white dwarfs are significantly more abundant in the galaxy. Thus, even if a sufficiently massive DM is unable to trigger a violent heating event within the lifetime of a WD, it could still ignite enough lighter WDs to affect the measured SN rate of ~ 0.3 per century. The DM-induced SN rate is estimated using the expected number of white dwarfs per galaxy $\sim 10^{10}$ and their mass distribution [11]. Simulations indicate that only WD masses heavier than $\sim 0.85 M_\odot$ will result in optically visible SN [4]. Therefore, most of the stars exploded in this manner will be in the mass range $\sim 0.85 - 1 M_\odot$, resulting in weaker SN than expected of typical Chandrasekhar mass WDs.

To summarize, a bound on DM parameters can be placed if either a single explosive event occurs during the lifetime of an observed star such as RX J0648.04418, or the SN rate due to such DM events throughout the galaxy exceeds the measured value. Note that for low-mass WDs dominated by photon diffusion, $\mathcal{E}_{\text{boom}}$ is a strong function of WD density. In [4] the central WD density is used to constrain black hole transits with the justification that the density is nearly constant for much of the star. The average density for WDs is typically a factor $\sim 10^{-2} - 10^{-1}$ less than the central density, although it is found that the WD density only changes by an $\mathcal{O}(1)$ fraction from the central value up to a distance $\sim R_{\text{WD}}/2$ [9]. Therefore the central density is a valid approximation as long as we consider heating events within this “modified” WD volume. For simplicity, we employ this approach.

B. Transit Constraints

In order to constrain a DM model through its transit interaction with a WD, we require that it satisfy the boom condition (13). This is given in terms of an LET, which parameterizes the ability for DM to release sufficient energy to the star in the form of SM particles. $(dE/dx)_{\text{LET}}$ for any realistic DM model would necessarily involve a sum over stellar targets along with species that could be produced, as well as an integral over the produced particle spectrum. However, we will consider a simplified interaction in which $\sigma_{Ni\epsilon}$ denotes the cross-section for DM to scatter off a stellar constituent (e.g. ions), producing N particles of SM species i and individual energy ϵ . If this were the only available channel for the DM to deposit energy, then the LET could be written as

$$\left(\frac{dE}{dx}\right)_{\text{LET}} = n_{\text{ion}} \sigma_{Ni\epsilon} N \epsilon. \quad (38)$$

The heating length for such a DM-SM scattering interaction is computed in Section III.

Additionally, consider the case that the LET $(dE/dx)_{\text{LET}}$ and DM stopping power $(dE/dx)_{\text{SP}}$ are equal—that is, the DM loses kinetic energy at the same rate as energy is deposited to the WD. While such a statement is certainly not true for all DM models (such as the Q-ball, which liberates binding energy rather than transferring kinetic energy), it provides a useful benchmark to express constraints. It is interesting to note that in this case combining the transit explosion condition (13) with (38) yields a lower bound on DM mass such that the DM is able to both penetrate the envelope *and* trigger an explosion:

$$m_\chi > \mathcal{E}_{\text{boom}} \left(\frac{R_{\text{env}}}{\lambda_T}\right) \left(\frac{\rho_{\text{env}}}{\rho_{\text{central}}}\right) \frac{1}{v_{\text{esc}}^2}. \quad (39)$$

For the typical parameters of a $1.25 M_\odot$ WD we find that the DM mass must be greater than $\sim 10^{28} \text{ GeV}$ to ensure a penetrating and explosive transit, taking the density of the WD non-degenerate envelope to be a nominal $\mathcal{O}(10^{-3})$ fraction of the central density [35]. In other words, if (39) were violated then the DM interaction is either not strong enough to ignite the WD or is so strong that the DM cannot penetrate the envelope without losing appreciable kinetic energy. We reiterate, however, that this bound is only applicable when the energy input to the WD is chiefly coming from the DM kinetic energy, rather than binding energy or other sources.

With the above schematic for a DM transit, we use the rates and heating lengths computed in previous sections to constrain the parameter $\sigma_{Ni\epsilon}$ as a function of DM mass m_χ . This is done in Figure 7 using the different classes of observation available and for representative choices of ϵ and SM species i released.

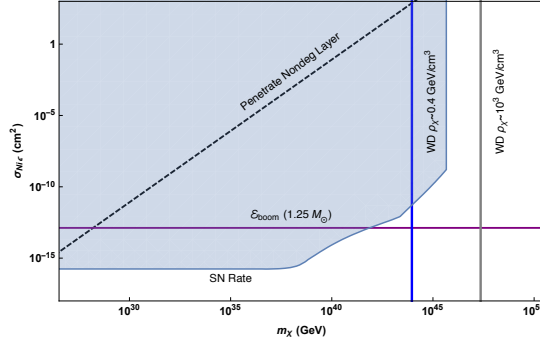


FIG. 7: Constraints on a DM-nuclei scattering cross-section to produce a single TeV photon. Bounds come from demanding that heating events satisfy (13) and occur at a rate (15) rapid enough to either ignite a single observed $1.25 M_{\odot}$ WD in its lifetime (local and galactic center) or exceed the measured SN rate in our galaxy.

C. Collision and Decay Constraints

In order to constrain a DM model through its annihilations or decays within a WD, we require that it satisfy the boom condition (16). Consider a simplified interaction where an annihilation or decay releases N particles of SM species i and individual energy ϵ . If we assume a fractional parameter $f_{\text{SM}} = 1$, this corresponds to the entire mass of DM being converted into SM products i , each with energy m_{χ}/N . These will deposit their energy and thermalize ions within a distance described in Section III.

With this schematic for DM-DM collisions, we use the rates and heating lengths computed in previous sections to constrain the cross section $\sigma_{\chi\chi}$ using the different classes of observation available and for representative choices of f_{SM} and SM species i released. This is done in Figure 8 for the wind scenario and Figure ?? for the capture scenario. In a similar manner, we constrain the lifetime τ_{χ} in Figures 9 and ??.

Complementary Limits It is important to note that there are additional limits on DM interactions of this kind, complementary to the limits placed from WDs. For instance, DM can annihilate or decay into ultra-high energy particles within our galactic halo and therefore contribute to the cosmic ray flux seen in terrestrial air shower detectors. As cosmic rays of energy greater than $\sim 10^{12}$ GeV have not yet been observed [14, 15], this places a concrete limit on DM interaction parameters $\sigma_{\chi\chi}$ and τ_{χ} which involve the release of such ultra-high energy particles. In theory a constraint may also be placed on lower-energy SM products from DM annihilations or decays, which would provide an additional source for the measured cosmic ray flux, although such a detailed analysis is beyond the scope of this work.

The cosmic ray constraint on DM is derived by requiring that the expected time for an event to strike earth is less than the lifetime of the detector ~ 10 yr. For a cosmic ray detector with area $\sim (50 \text{ km})^2$ [14], we find that the cosmic ray bounds are weaker than the WD bounds except in the DM decay “wind scenario”, where the cosmic rays bounds are comparable within a couple orders of magnitude to those due to the observation of a local WD. This coincidence is simply a consequence of the similar “space-time volumes” of the two systems. A cosmic ray detector sees events within a space-time volume $\sim (R_{\text{det}}^2 R_{\text{halo}} \times 10 \text{ yr})$ which is comparable to the WD space-time volume for decay events $\sim (R_{\text{WD}}^3 \times 10^9 \text{ yr} \times 10)$, including the factor of 10 gravitational enhancement.

In addition, there are various cosmological bounds on DM interactions. By requiring that the galactic halo has not diminished by more than an $\mathcal{O}(1)$ factor during its lifetime, we constrain $\sigma_{\chi\chi}/m_{\chi} \lesssim \text{barn/GeV}$, regardless of the precise details of the collision. This is similar in magnitude to the DM self-interaction bounds from colliding galaxy clusters [17]. The cosmological bound on DM lifetime $\tau_{\chi} \gtrsim 100 \text{ Gyr}$ is also independent of the nature of the decay products (see [16] for details). Since the limits imposed by the WD scale as $\sigma_{\chi\chi} \propto m_{\chi}^2$ and $\tau_{\chi} \propto m_{\chi}^{-1}$, there will necessarily be a sufficiently large DM mass for which the above cosmological considerations are the more stringent constraints on its interactions. This occurs for DM masses $m_{\chi} \sim 10^{25} - 10^{30} \text{ GeV}$.

VI. Q-BALLS

Having derived constraints on generic models of ultra-heavy DM, we turn towards a concrete example. In various supersymmetric extensions of the SM, non-topological solitons called Q-balls can be produced in the early universe [19, 20]. If these Q-balls were stable, they would comprise a component of the DM today. For gauge-mediated models

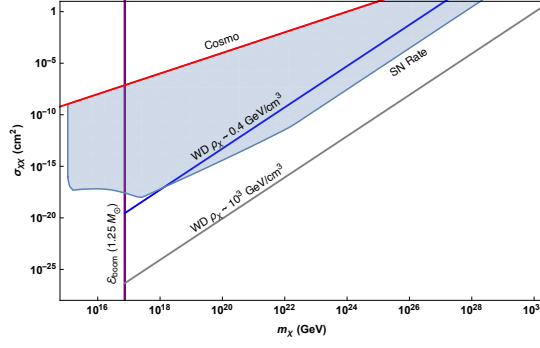


FIG. 8: Constraints on DM-DM collision cross-section into photons with individual energy $\epsilon > 10$ MeV and $f_{\text{SM}} = 1$. Bounds come demanding that heating events satisfy (16) and occur at a rate (17) (“wind scenario”) rapid enough to either ignite a single observed $1.25 M_{\odot}$ WD in its lifetime (local and galactic center) or exceed the measured SN rate in our galaxy.

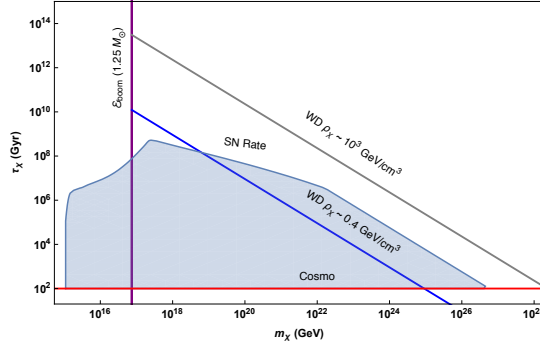


FIG. 9: Constraints on DM decay lifetime into photons with individual energy $\epsilon > 10$ MeV and $f_{\text{SM}} = 1$. Bounds come demanding that heating events satisfy (16) and occur at a rate (18) (“wind scenario”) rapid enough to either ignite a single observed $1.25 M_{\odot}$ WD in its lifetime (local and galactic center) or exceed the measured SN rate in our galaxy.

with flat scalar potentials, the Q-ball mass and radius are given by

$$M_Q \sim m_S Q^{3/4}, \quad R_Q \sim m_S^{-1} Q^{1/4}, \quad (40)$$

where m_S is related to the scale of supersymmetry breaking, and Q is the global charge of the Q-ball—in our case, baryon number. The condition $M_Q/Q < m_p$ ensures that the Q-ball is stable against decay to nucleons. When an electrically neutral baryonic Q-ball interacts with a nucleon, it absorbs its baryonic charge and induces the dissociation of the nucleon into free quarks. During this proton decay-like process, $\sim \text{GeV}$ of energy is released through the emission of 2–3 pions [21]. We assume that for each Q-ball collision, there is equal probability to produce π^0 and π^\pm under the constraint of charge conservation. Note that a sufficiently massive Q-ball will become a black hole if $R_Q \lesssim GM_Q$. In the model described above, this translates into a condition $(M_{\text{pl}}/m_S)^4 \lesssim Q$.

We now determine the explosiveness of a Q-ball transit. As in Section V, this process is described by the parameter

$$\left(\frac{dE}{dx} \right)_{\text{LET}} \sim n_{\text{ion}} \sigma_Q N \epsilon, \quad (41)$$

where the nuclear collision results in $N \sim 30$ pions released, each with kinetic energy $\epsilon \sim 500$ MeV. These pions induce hadronic showers which terminate in low-energy hadrons that rapidly transfer their energy to ions via elastic scatters, as discussed in Section III. Thus the Q-ball transit has a heating length within the trigger size, and the Q-ball cross-section necessary to trigger runaway fusion is given by equations (13) and (41):

$$\sigma_Q \gtrsim \frac{1}{n_{\text{ion}}} \frac{\mathcal{E}_{\text{boom}}}{\lambda_T} \left(\frac{1}{10 \text{ GeV}} \right). \quad (42)$$

We see $\sigma_Q \approx 10^{-12} \text{ cm}^2$ is sufficient to blow up a $\sim 1.25 M_{\odot}$ WD. The cross-section for this interaction is approximately geometric

$$\sigma_Q \sim \pi R_Q^2, \quad (43)$$

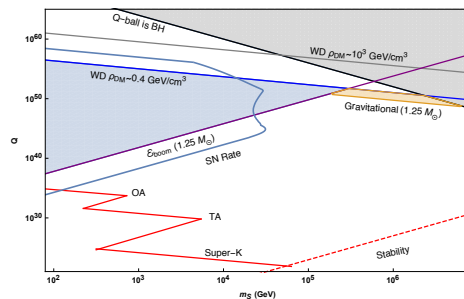


FIG. 10: Constraints on baryonic Q-balls from transits of a $\sim 1.25 M_{\odot}$ WD in the galactic center, $\rho_{\chi} \sim 10^3 \text{ g/cm}^3$. We include constraints from heating by strong interactions with nuclei and gravitational interactions (dynamical friction). Also shown are the limits from Super-K and the OA, TA cosmic ray detectors, extracted from [22].

and so $Q \gtrsim 10^{42} (m_S/\text{TeV})^4$ can be adequately constrained from the observation of a single, heavy WD. Note that the Q-ball interaction described above results in minimal slowing or transfer of kinetic energy for Q-balls this massive, so transits will easily penetrate the non-degenerate WD layer (12).

The strongest previous constraints on Q-balls come from Super-Kamiokande as well as air fluorescence detectors of cosmic rays [22]. However, the constraints due to white dwarfs are in a fundamentally complementary region of parameter space. These are plotted in Figure 10. As a comparison, the combined limits from Super-K and the OA, TA cosmic ray detectors are shown in red. We have also included the constraints from a WD which result from considering gravitational heating during a Q-ball transit, as in [4].

VII. DISCUSSION

The detection of ultra-heavy DM is an open problem which will likely require a confluence of astrophysical probes. Here we present a comprehensive guide to containing these DM candidates through annihilates, decays, and transits within a WD that release sufficient SM energy to trigger a type 1a supernova. In particular, we calculate the energy loss of high-energy particles due to SM interactions within the WD medium and determine the conditions for which a general energy deposition will heat a WD and ignite thermonuclear runaway. The formalism provided will enable WDs to be applied as detectors for any DM models capable of heating the star through non-gravitational interactions, and as a concrete example we are able to place bounds on supersymmetric Q-ball DM over a wide region of parameter space.

In general, the phenomenology of such a DM-induced event will be the ignition of sub-Chandrasekhar mass progenitors. This raises the tantalizing possibility that DM encounters with a WD can act as an alternative explosion mechanism and progenitor system for type 1a SN. For decades, standard lore has been that type 1a SN are caused by accretion onto carbon-oxygen white dwarfs in binary systems that reach the critical $\sim 1.4 M_{\odot}$ Chandrasekhar mass limit. Nevertheless, it is well-known that such a mechanism cannot account for all observed type 1a SN. Recent observations [23, 24] suggest that an $\mathcal{O}(1)$ fraction of the observed type 1a SN appear to have sub-Chandrasekhar progenitors. A leading explanation for this phenomenon is the detonation of a surface layer of helium which drives a shock into the interior of a sub-Chandrasekhar-mass WD [25, 26]. However, in light of the lack of understanding of DM and its interactions, it is worthwhile to consider whether a DM-WD encounter may also give rise to type 1a SN progenitor.

A. PARTICLE STOPPING IN A WHITE DWARF

Here we provide a more detailed analysis of the stopping power (energy loss per distance traveled) of high-energy SM particles in a carbon-oxygen WD due to electromagnetic and strong interactions. We consider incident electrons, photons, pions, and nucleons with kinetic energy greater than an MeV.

A. WD Medium

For the WD masses that we consider, the stellar medium consists of electrons and fully-ionized carbon nuclei with densities in the range $n_e = Zn_{\text{ion}} \sim 10^{31} - 10^{33} \text{ cm}^{-3}$ where $Z = 6$. The internal temperature is $T \sim \text{keV}$ [35]. The

electrons are a degenerate and predominantly relativistic free gas, with Fermi energy

$$E_F \sim (3\pi^2 n_e)^{1/3} \sim 1 - 10 \text{ MeV}. \quad (44)$$

The carbon ions, however, are non-degenerate and do not form a free gas. The plasma frequency due to ion-ion Coulomb interactions is given by

$$\Omega_p = \left(\frac{4\pi n_{\text{ion}} Z^2 \alpha}{m_{\text{ion}}} \right)^{1/2} \sim 1 - 10 \text{ keV}, \quad (45)$$

where m_{ion} is the ion mass. Finally, the medium also contains thermal photons, though these are never significant for stopping particles as the photon number density $n_\gamma \sim T^3$ is much smaller than that of electrons or ions.

B. Nuclear Interactions

a. Elastic Scattering of Hadrons. Hadrons with energy less than the nuclear binding energy $E_{\text{nuc}} \sim 10 \text{ MeV}$ will predominantly stop due to elastic nuclear scatters with ions. These are hard scatters, resulting in a stopping power

$$\frac{dE}{dx} \sim n_{\text{ion}} \sigma_{\text{el}} \left(\frac{m}{m_{\text{ion}}} \right) E \quad (46)$$

for a hadron of mass $m \ll m_{\text{ion}}$ and kinetic energy E . σ_{el} is the elastic nuclear scattering cross-section, which is of order $\sim b$ at these energies and drops to $\sim 0.1 b$ above 10 MeV [33], ignoring the presence of various nuclear resonances in the range 1 MeV to 10 MeV.

b. Inelastic Scattering of Hadrons. For energies above E_{nuc} , the stopping of hadrons is dominated by inelastic nuclear scatters. In such a collision, an incoming hadron interacts with one or more nucleons to produce a $\mathcal{O}(1)$ number of additional hadrons which approximately split the initial energy. At incident energy greater than $\sim \text{GeV}$, the majority of secondary hadrons are pions with transverse momenta $\sim 100 \text{ MeV}$ [33]. Below $\sim \text{GeV}$, it is found that roughly equal fractions of protons, neutrons, and pions are produced in each collision [34]. We will thus have a roughly collinear shower terminating at an energy $\sim 10 \text{ MeV}$ which consists of pions for most of the shower's development and converts to an mix of pions and nucleons in the final decade of energy. This cascade is described by a radiative stopping power

$$\frac{dE}{dx} \sim n_{\text{ion}} \sigma_{\text{inel}} E, \quad (47)$$

where the inelastic nuclear cross-section σ_{inel} is given by $\sigma_{\text{inel}} \approx 100 \text{ mb}$ and is roughly constant in energy [33]. The total length of the shower is only logarithmically dependent on the initial hadron energy E ,

$$X_{\text{had}} \sim \frac{1}{n_{\text{ion}} \sigma_{\text{inel}}} \log \left(\frac{E}{10 \text{ MeV}} \right). \quad (48)$$

c. Photonuclear Interactions. Photons of energy greater than 10 MeV can also strongly interact with nuclei through the production of virtual quark-antiquark pairs. This is the dominant mode of photon energy loss at high energy. The photonuclear scatter destroys the photon and fragments the nucleus, producing secondary hadrons in a shower analogous to that described above. The photonuclear cross-section $\sigma_{\gamma A}$ is roughly given by $\sigma_{\gamma A} \approx \alpha \sigma_{\text{inel}}$, again ignoring the nuclear resonances that occur for $E \lesssim \text{GeV}$. [33] For $E \gtrsim \text{GeV}$, $\sigma_{\gamma A}$ is likely a slowly increasing function of energy due to the coherent interaction of the photon over multiple nucleons [31], however, instead of extrapolating this behavior we conservatively take a constant photonuclear cross-section $\sigma_{\gamma A} \approx 1 \text{ mb}$.

d. Electronuclear Interactions. Electrons can similarly lose energy to nuclei by radiating a virtual photon that undergoes a photonuclear scatter, which indeed provides the dominant energy loss for high energy electrons. The cross-section for this process is roughly given by the photonuclear cross-section, scaled by a factor representing the probability to radiate such a photon. This can be estimated with the Weizsacker-Williams approximation, which gives a stopping power that is suppressed from the photonuclear result by α but enhanced by an $\mathcal{O}(10)$ kinematic factor [31]:

$$\frac{dE}{dx} \sim 10^{-3} \cdot n_{\text{ion}} \sigma_{\text{inel}} E. \quad (49)$$

Unlike the photonuclear interaction, the electronuclear event is a radiative process that preserves the original electron while leaving hadronic showers in its wake.

C. Radiative Processes

Electromagnetic showers due to successive bremsstrahlung and pair production events off carbon ions are the dominant stopping mechanisms for intermediate-energy electrons and photons. Both of these processes result in radiative stopping powers, expressed semi-classically as [36]

$$\left(\frac{dE}{dx}\right) \sim \frac{E}{X_0}, \quad X_0^{-1} = 4n_{\text{ion}}Z^2 \frac{\alpha^3}{m_e^2} \log \Lambda. \quad (50)$$

X_0 is the radiation length, and $\log \Lambda$ is a Coulomb form factor given by the range of effective impact parameters b :

$$\Lambda = \frac{b_{\text{max}}}{b_{\text{min}}} \sim \lambda_{\text{TF}} m_e. \quad (51)$$

The maximal impact parameter is set by the plasma screening length and the minimum by the electron mass, below which the semi-classical description breaks down. For the highest WD densities, we may indeed have that $\Lambda \lesssim 1$, in which case equation (??) ought to be replaced by a quantum mechanical result, such as the Bethe-Heitler formula [37]. This still results in a radiative stopping power, and so for simplicity we employ equation (??) and take $\log \Lambda \sim \mathcal{O}(1)$ for all WD densities.

a. LPM Suppression A radiative event involving momentum transfer q to an ion must, quantum mechanically, occur over a length $\sim q^{-1}$. All ions within this region contribute to the scattering of the incident particle, and for sufficiently small q this results in a decoherence that suppresses the formation of photons or electron-position pairs. This is the ‘‘Landau-Pomeranchuk-Midgal’’ (LPM) effect. The momentum transfer q in a given event decreases with increasing incident particle energy, and so the LPM effect will suppress radiative processes for energies greater than some scale E_{LPM} . This can be calculated semi-classically [36],

$$E_{\text{LPM}} = \frac{m_e^2 X_0 \alpha}{4\pi} \approx 1 \text{ MeV} \left(\frac{10^{32} \text{ cm}^{-3}}{n_{\text{ion}}} \right). \quad (52)$$

which is quite small due to the high ion density in the WD. The stopping power for bremsstrahlung and pair production at energies $E > E_{\text{LPM}}$ is

$$\left(\frac{dE}{dx}\right)_{\text{LPM}} \sim \frac{E}{X_0} \left(\frac{E_{\text{LPM}}}{E}\right)^{1/2} \quad E > E_{\text{LPM}}. \quad (53)$$

In addition to the LPM effect, soft bremsstrahlung may be suppressed in a medium as the emitted photon acquires an effective mass of order the plasma frequency Ω_p . However, for high-energy electrons this dielectric suppression only introduces a minor correction to (53), in which soft radiation is already suppressed [36].

Note that the LPM effect is less significant for higher-order electromagnetic processes since these generally involve larger momentum transfers for the same final-state kinematics. Thus when the suppression factor exceeds $\mathcal{O}(\alpha)$, these interactions should be considered. For instance, the energy loss due to electron direct pair production $eN \rightarrow e^+ e^- eN$ and is found to exceed that of bremsstrahlung at an energy $\sim 10^8 \text{ GeV}$ [31]. At such high energies the stopping power for photons/electrons is dominated by photonuclear and electronuclear interactions anyway.

D. Elastic EM Scattering

a. Coulomb Scattering off Carbon Ions. Coulomb collisions with ions provide the dominant mechanism by which electrons with energy $1 \text{ MeV} \lesssim E \lesssim 10 \text{ MeV}$ thermalize ions. In this scenario we may treat the ions as stationary and ignore their recoil during collisions. The nuclear charge will be screened by the mobile electrons of the medium, so incident particles will scatter via a potential

$$V(\mathbf{r}) = \frac{Z\alpha}{r} e^{-\lambda_{\text{TF}} r}. \quad (54)$$

The screening length λ_{TF} is given in the Thomas-Fermi approximation by [29]

$$\lambda_{\text{TF}}^2 = \frac{E_F}{6\pi\alpha n_e} \sim \frac{1}{\alpha n_e^{2/3}} \quad (55)$$

where E_F is the electron Fermi energy. This plasma screening suppresses scatters with momentum transfers below $\sim \lambda_{\text{TF}}^{-1}$, corresponding to a minimal energy transfer of $\omega_{\min} = \lambda_{\text{TF}}^{-2}/2m_{\text{ion}}$. Ions may in principle also cause screening through lattice distortion, however this may be ignored as the sound speed of the lattice $c_s \sim 10^{-2}$ is much smaller than the speed of an incident relativistic electron. Using the Born approximation, we have a cross-section for energy transfer ω

$$\frac{d\sigma}{d\omega} = \frac{2\pi Z^2 \alpha^2}{m_{\text{ion}} \beta^2} \frac{1}{(\omega + \omega_{\min})^2} \quad (56)$$

and a stopping power

$$\begin{aligned} \frac{dE}{dx} &= \int_0^{\omega_{\max}} d\omega n_{\text{ion}} \frac{d\sigma}{d\omega} \omega \\ &\approx \frac{2\pi n_{\text{ion}} Z^2 \alpha^2}{m_{\text{ion}} \beta^2} \log \left(\frac{\omega_{\max}}{\omega_{\min}} \right) \end{aligned} \quad (57)$$

where the second line is valid if $\omega_{\max} \gg \omega_{\min}$. ω_{\max} is the maximum possible energy transfer. This may be due to 4-momentum conservation, or in the case of incident electrons, the impossibility of scattering to a final energy less than E_F . 4-momentum conservation sets an upper bound ω_{kin} , which for a stationary target is

$$\omega_{\text{kin}} = \frac{2m_{\text{ion}} p^2}{m_{\text{ion}}^2 + m^2 + 2Em_{\text{ion}}} \quad (58)$$

with p , E the incoming momentum and energy. The Fermi upper bound is simply $\omega_F = E - E_F$ so for incident electrons we take $\omega_{\max} = \min(\omega_{\text{kin}}, \omega_F)$.

For scatters that transfer energy less than the plasma frequency Ω_p , one may be concerned about phonon excitations. We estimate this by treating each ion as an independent oscillator with frequency Ω_p (an Einstein solid) and compute the stopping power due to scatters which excite a single oscillator quanta. There are two key differences between this and the free ion case: incident particles must transfer an energy Ω_p and the cross-section to transfer momentum q is suppressed by a factor $q^2/2m_{\text{ion}}\Omega_p = \omega_{\text{free}}/\Omega_p$. ω_{free} is the energy transfer that would accompany a free ion scatter with momentum transfer q . The resulting stopping power is unchanged from the free case (57), as the increased energy transfer compensates for the suppressed cross-section:

$$d\sigma \cdot \omega \sim d\sigma_{\text{free}} \frac{\omega_{\text{free}}}{\Omega_p} \cdot \Omega_p \sim d\sigma_{\text{free}} \cdot \omega_{\text{free}}. \quad (59)$$

Finally, we note that for more energetic incident particles the cross-section (56) should be replaced to account for the recoil of the ion during collisions. In these scenarios, however, this stopping power is far subdominant to hadronic or electromagnetic showers.

b. Coulomb Scattering off Electrons. The scattering of incident electrons with the degenerate electron sea determines the termination energy of electromagnetic showers, and so we focus here on that scenario. This calculation demands two considerations not present when scattering off ions: the targets are not stationary and they require a threshold energy transfer in order to be scattered out of the Fermi sea. In the scenario of interest, however, these do not result in a parametrically different stopping power than was found for ions in equation (57).

For incident momenta much greater than the Fermi momentum, the relative velocity is of order the incident velocity and the deflection of the incident particle will generally be small. It is reasonable then that scattering proceeds, up to $\mathcal{O}(1)$ factors, as though a heavy incident particle is striking a light, stationary target. The cross-section is then given by the usual result,

$$\frac{d\sigma}{d\omega} \approx \frac{2\pi \alpha^2}{E_F} \frac{1}{\omega^2}, \quad (60)$$

where we have accounted for the target's motion by replacing its mass with the relativistic inertia $\sqrt{m_e^2 + p^2} \approx E_F$. We have ignored plasma screening, as Pauli-blocking will provide a more stringent cutoff on soft scatters in this case. Scatters which transfer an energy $\omega \leq E_F$ will have a suppressed contribution to the stopping power as they can only access a fraction of the Fermi sea. For incident energies $E \gg E_F$ it is sufficient to ignore these suppressed scatters, i.e.,

$$\begin{aligned} \frac{dE}{dx} &= \int_{E_F}^{\omega_{\max}} d\omega n_e \frac{d\sigma}{d\omega} \omega \\ &\approx \frac{2\pi n_e \alpha^2}{E_F} \log \left(\frac{\omega_{\max}}{E_F} \right) \end{aligned} \quad (61)$$

where, as above, $\omega_{\max} = \min(\omega_{\text{kin}}, \omega_F)$. This derivation is admittedly quite heuristic, and so it has been checked with a detailed numerical calculation accounting fully for the target's motion and degeneracy. Equation (61) is indeed a good approximation to the stopping power for incident energies larger than the Fermi energy.

c. Compton Scattering For incident photon energies less than the Fermi energy, the dominant stopping is provided by Compton scatters with degenerate electrons. This stopping power differs parametrically from its usual form due to the target electron motion and degeneracy.

Consider an incident photon with energy $k \leq E_F$. Compton scatters will only occur off electrons moving roughly collinear with the photon momentum - a head-on collision would result in an energy loss for the electron, which is forbidden by Pauli exclusion. In the electron rest frame these collinear scatters are Thompson-like, and so the photon energy loss is dominated by backward scatters. For relativistic electrons near the Fermi surface, these scatters transfer an energy

$$\omega \approx k \left(1 - \frac{m_e^2}{4E_F^2} \right) \sim k. \quad (62)$$

The cross-section can be taken in the electron rest frame, $\sigma_T \sim \alpha^2/m_e^2$, along with an ‘aiming’ factor $1/4\pi$ to account for the restriction to initially parallel trajectories. Finally, for $k \ll E_F$ only those electrons near the top of the Fermi sea are available to scatter, so the photon interacts with an effective electron density of

$$n_{\text{eff}} = \int_{E_F-k}^{E_F} g(E) dE \approx 3n_e \frac{k}{E_F} \quad (63)$$

where $g(E)$ is the Fermi density of states. This gives a stopping power

$$\frac{dk}{dx} \approx \frac{\alpha^2 n_e k^2}{m_e^2 E_F}. \quad (64)$$

Acknowledgements

We would like to thank Keisuke Harigaya, Spencer Klein, Jacob Leedom, Robert McGehee, and Lian-Tao Wang for stimulating discussions.

-
- [1] K. Griest, A. M. Cieplak and M. J. Lehner, *Astrophys. J.* **786**, no. 2, 158 (2014) doi:10.1088/0004-637X/786/2/158 [arXiv:1307.5798 [astro-ph.CO]].
 - [2] D. S. Akerib *et al.* [LUX Collaboration], *Phys. Rev. Lett.* **118**, no. 2, 021303 (2017) doi:10.1103/PhysRevLett.118.021303 [arXiv:1608.07648 [astro-ph.CO]].
 - [3] R. Agnese *et al.* [SuperCDMS Collaboration], arXiv:1708.08869 [hep-ex].
 - [4] P. W. Graham, S. Rajendran and J. Varela, *Phys. Rev. D* **92**, no. 6, 063007 (2015) [arXiv:1505.04444 [hep-ph]].
 - [5] F. X. Timmes and S. E. Woosley, *Astro. Phys. Journal* **396**, 649 (1992).
 - [6] L. R. Gasques, A. V. Afanasjev, E. F. Aguilara, M. Beard, L. C. Chamon, P. Ring, M. Wiescher and D. G. Yakovlev, *Phys. Rev. C* **72**, 025806 (2005) [astro-ph/0506386].
 - [7] F. X. Timmes, [link](#)
 - [8] J. A. Formaggio and G. P. Zeller, *Rev. Mod. Phys.* **84**, 1307 (2012) [arXiv:1305.7513 [hep-ex]].
 - [9] S. Chandrasekhar, “An Introduction to the Study of Stellar Structure”, University of Chicago press (1939).
 - [10] S. Mereghetti, arXiv:1302.4634 [astro-ph.HE].
 - [11] S. J. Kleinman, S. O. Kepler, D. Koester, I. Pelisoli *et al.*, *Astrophys. J. Suppl.* **204**, article id. 5, 14 pp. (2013)
 - [12] K. Perez, C. J. Hailey, F. E. Bauer, *et al.*, *Nature* **520**, 646 (2015)
 - [13] F. Nesti and P. Salucci, *JCAP* **1307**, 016 (2013) [arXiv:1304.5127 [astro-ph.GA]].
 - [14] A. Aab *et al.* [Pierre Auger Collaboration], *JCAP* **1508**, 049 (2015) [arXiv:1503.07786 [astro-ph.HE]].
 - [15] T. Abu-Zayyad *et al.* [Telescope Array Collaboration], *Astrophys. J.* **768**, L1 (2013) [arXiv:1205.5067 [astro-ph.HE]].
 - [16] V. Poulin, P. D. Serpico and J. Lesgourgues, *JCAP* **1608**, no. 08, 036 (2016) [arXiv:1606.02073 [astro-ph.CO]].
 - [17] S. W. Randall, M. Markevitch, D. Clowe, A. H. Gonzalez and M. Bradac, *Astrophys. J.* **679**, 1173 (2008) [arXiv:0704.0261 [astro-ph]].
 - [18] N. Padmanabhan and D. P. Finkbeiner, *Phys. Rev. D* **72**, 023508 (2005) [astro-ph/0503486].
 - [19] S. R. Coleman, *Nucl. Phys. B* **262**, 263 (1985) Erratum: [*Nucl. Phys. B* **269**, 744 (1986)].

- [20] A. Kusenko and M. E. Shaposhnikov, Phys. Lett. B **418**, 46 (1998) [hep-ph/9709492].
- [21] A. Kusenko, V. Kuzmin, M. Shaposhnikov, P. G. Tinyakov, Phys. Rev. Lett. **80**, 15 (1998) [hep-ph//9712212].
- [22] M. Dine and A. Kusenko, Rev. Mod. Phys. **76**, 1 (2003) [hep-ph/0303065].
- [23] R. Scalzo *et al.* [Nearby Supernova Factory Collaboration], Mon. Not. Roy. Astron. Soc. **440**, no. 2, 1498 (2014) [arXiv:1402.6842 [astro-ph.CO]].
- [24] R. A. Scalzo, A. J. Ruiter and S. A. Sim, Mon. Not. Roy. Astron. Soc. **445**, no. 3, 2535 (2014) [arXiv:1408.6601 [astro-ph.HE]].
- [25] S. E. Woosley and T. A. Weaver, Astrophysical Journal **423**, pp.371-379 (1994).
- [26] M. Fink, W. Hillebrandt and F. K. Roepke, Astron. Astrophys. [Astron. Astrophys. **476**, 1133 (2007)] [arXiv:0710.5486 [astro-ph]].
- [27] B. Rossi, "High Energy Particles", Prentice-Hall, Inc., Englewood Cliffs, NJ (1952).
- [28] J. D. Jackson, "Classical Electrodynamics", 3rd edition, John Wiley and Sons, New York, (1998).
- [29] S. L. Shapiro and S. A. Teukolsky, "Black Holes, White Dwarfs, and Neutron Stars", Wiley (1983).
- [30] S. Klein, Rev. Mod. Phys. **71**, 1501 (1999) [hep-ph/9802442].
- [31] L. Gerhardt and S. R. Klein, Phys. Rev. D **82**, 074017 (2010) [arXiv:1007.0039 [hep-ph]].
- [32] S. Klein, private communication
- [33] S. Tavernier, "Experimental Techniques in Nuclear and Particle Physics", Springer (2010).
- [34] T. S. H. Lee and R. P. Redwine, Annu. Rev. Nucl. Part. Sci **52**, pp.23-63 (2002)
- [35] R. Kippenhahn and A. Weigert, "Stellar Structure and Evolution, Springer (1994).
- [36] S. Klein, Rev. Mod. Phys. **71**, 1501 (1999) [hep-ph/9802442].
- [37] H. Bethe and W. Heitler Proc. R. Soc. Lond. A 1934 146 83-112